

Observations of Ultracool White Dwarfs

B. R. Oppenheimer

Astronomy Department, University of California, Berkeley, CA 94720-3411, USA

`bro@astron.berkeley.edu`

D. Saumon

Department of Physics and Astronomy, Vanderbilt University, Nashville, TN 37235, USA

S. T. Hodgkin

Institute for Astronomy, Cambridge University, Madingley Road, Cambridge, CB3 0HA, UK

R. F. Jameson

Department of Physics and Astronomy, University of Leicester, University Road, Leicester, LE1 7RH, UK

N. C. Hambly

Institute for Astronomy, University of Edinburgh, Blackford Hill, Edinburgh, EH9 3HJ, UK

G. Chabrier

C. R. A. L., Ecole Normale Supérieure, 69364 Lyon Cedex 07, France

A. V. Filippenko, A. L. Coil

Astronomy Department, University of California, Berkeley, CA 94720-3411, USA

and

M. E. Brown

Department of Geological and Planetary Sciences, California Institute of Technology, 170-25, Pasadena, CA 91125, USA

ABSTRACT

We present new spectroscopic and photometric measurements of the white dwarfs LHS 3250 and WD 0346+246. Along with F351–50, these white dwarfs are the coolest ones known, all with effective temperatures below 4000 K. Their membership in the Galactic halo population is discussed, and detailed comparisons of all three objects with new atmosphere models are presented. The new models consider the effects of mixed H/He atmospheres and indicate that WD 0346+246 and F351–50 have predominantly helium atmospheres with only traces of hydrogen. LHS 3250 may be a double degenerate whose average radiative temperature is between 2000 and 4000 K, but the new models fail to explain this object.

Subject headings: stars: individual (LHS 3250, WD 0346+246, F351–50) — stars: white dwarfs

1. Introduction

The recent discovery of three white dwarfs with temperatures below 4000 K (Hambly et al. 1997, 1999; Harris et al. 1999; Hodgkin et al. 2000; Ibata et al. 2000) shows that extremely cool white dwarfs have blue colors in the infrared and may peak in flux density at wavelengths as short as $0.6 \mu\text{m}$. The spectral energy distributions (SEDs) of these cool white dwarfs deviate from the black body spectrum by up to four magnitudes in the infrared because of the presence of deep absorption due to collisionally induced dipole moments in H_2 molecules (commonly referred to as H_2 collision induced absorption or H_2 CIA; Borysow & Frommhold (1990)). Theoretical predictions of this phenomenon by Bergeron et al. (1994), Saumon & Jacobson (1999), and Hansen (1999) have now been unambiguously confirmed in LHS 1126 (Bergeron et al. 1995a), LHS 3250 (Harris et al. 1999) and WD 0346+246 (Hodgkin et al. 2000), which has been spectroscopically observed in the infrared. The SED demonstrates that the widespread assumption that optical and infrared colors monotonically redden with decreasing effective temperature is wrong.

We present here a compilation of new and previously published observations of three “ultra-cool” white dwarfs, WD 0346+246, LHS 3250, and F351–50. Our new observations of WD 0346+246 and LHS 3250 include spectra and photometry from U through K band, the wavelength region in which these stars are brightest. All of these objects were discovered because of their high proper motions and all clearly exhibit extreme flux deficits in the near-infrared. Furthermore, the measured parallaxes and proper motions enable a discussion of their membership in the Galaxy’s halo population.

To complement the observational work, we present synthetic spectra of such white dwarfs. We expand the models of Saumon & Jacobson (1999) by considering atmospheres of mixed hydrogen and helium composition. We use these new models to fit our new data along with previous parallax measurements of WD 0346+246 (Hambly et al. 1999) and LHS 3250 (Harris et al. 1999). Such fits should ideally provide complete physical solutions for these white dwarfs. However, only the spectra of WD 0346+246 and

F351–50 (published in Ibata et al. (2000) without a parallax measurement) can be explained by the new models. LHS 3250 remains an enigma, but we discuss the general properties in depth. For WD 0346+246, because the parallax is known, we derive the luminosity (L), effective temperature (T_{eff}), mass (M), and radius (R).

2. Observations

Our new observations of LHS 3250 and WD 0346+246 spanned more than a year and involved multiple instruments and telescopes. For WD 0346+246, we have re-reduced our infrared spectrum (first presented in Hodgkin et al. (2000)), obtained a new optical spectrum and measured U and B band photometry. For LHS 3250, we have obtained spectra spanning 0.8 to $2.5 \mu\text{m}$. The photometric measurements are shown in Table 1. Figure 1 presents the photometry and spectroscopy of WD 0346+246, and Figure 2 plots the new spectroscopy of LHS 3250 along with the Harris et al. (1999) spectrum and photometry. In our subsequent analysis sections we additionally consider the spectrum of F351–50 from Ibata et al. (2000).

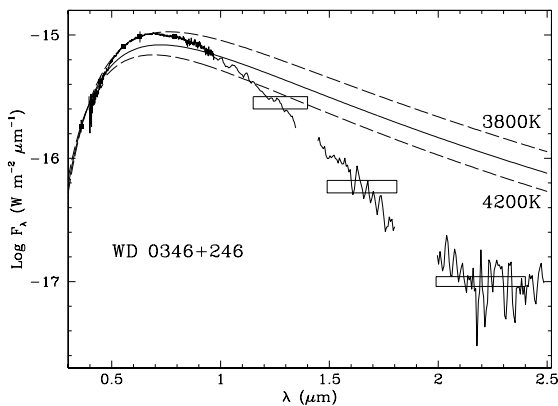


Fig. 1.— Spectra and photometry of WD 0346+246. The open boxes indicate the infrared photometry. Their width corresponds to the wavelength range of the filter and the height corresponds to the uncertainty in flux density. The small closed squares mark the optical photometric measurements. Those points without error bars have errors smaller than the size of the squares. The spectral data have been smoothed over 3 pixels (approximately 1 resolution element). Three black body spectra (at 3800, 4000 and 4200 K) are also plotted to show the fitting used in §5 to the wavelength region below $0.5 \mu\text{m}$. They also clearly illustrate the strong infrared suppression.

TABLE 1
PHOTOMETRY OF WD 0346+246

Band	λ_{eff} (μm)	Mag.	f_{λ} ($\text{W m}^{-2} \mu\text{m}^{-1}$)	Lum. (L_{\odot})
<i>U</i>	0.3686	20.8 ± 0.1	1.81×10^{-16}	5.0×10^{-7}
<i>B</i>	0.4310	20.5 ± 0.1	4.14×10^{-16}	1.6×10^{-6}
<i>V</i>	0.5405	19.06 ± 0.01	8.51×10^{-16}	2.5×10^{-6}
<i>R</i>	0.6314	18.30 ± 0.08	1.02×10^{-15}	3.0×10^{-6}
<i>I</i>	0.7927	17.54 ± 0.02	1.08×10^{-15}	4.4×10^{-6}
<i>J</i>	1.2117	17.60 ± 0.05	2.79×10^{-16}	1.7×10^{-6}
<i>H</i>	1.6226	18.2 ± 0.1	5.93×10^{-17}	4.5×10^{-7}
<i>K</i>	2.1750	19.0 ± 0.1	9.97×10^{-18}	1.0×10^{-7}

NOTE.—According to the synthetic spectra (§6), the total luminosity of this object is about 15% higher than the sum of the numbers in the last column.

2.1. WD 0346+246

Hambly et al. (1997) presented an optical spectrum of WD 0346+246 which fell short of reaching $1.0 \mu\text{m}$. With the infrared spectrum in Hodgkin et al. (2000), a gap in the data set persisted between 0.8 and $1.0 \mu\text{m}$. The Hodgkin et al. (2000) infrared spectrum seemed to indicate the presence of a sharp peak in the spectrum somewhere in this gap. The Hambly et al. (1997) spectrum was about 0.1 mag discrepant with their optical photometry as well. With this in mind, we revisited the reduction of the infrared spectrum and obtained a new optical spectrum with careful flux calibration independent of any imaging photometric observations.

The new reduction of the infrared spectral data previously published in Hodgkin et al. (2000) (taken February 1999 at the Keck I 10-m telescope with the Near Infrared Camera, NIRC; Matthews & Soifer (1994)) revealed an error in the spectrophotometric calibration which caused a peak near $1.0 \mu\text{m}$. The error only affected the spectrum in the Z_{CIT} band and minimally in the J band. The error was due to an incomplete removal of the spectral shape of the standard star. This is a broad effect and introduced no spurious, fine features. Upon correction, the optical

and near-infrared spectra agree. Furthermore, the infrared spectrum agrees perfectly with the new, more carefully calibrated, optical spectrum described below.

The new optical spectrum of WD 0346+246 was taken with the Low-Resolution Imaging Spectrometer (LRIS; (Oke et al. 1995)) on the Keck II 10-m telescope on 15 December 1999 UT under clear conditions and $0.7''$ seeing. The spectrum was obtained with a low-dispersion grating and two different blocking filters to acquire the full wavelength range from 0.39 to $1.0 \mu\text{m}$. The 150 l mm^{-1} grating blazed at $0.75 \mu\text{m}$ in conjunction with the $1.0''$ slit provided an average dispersion of $\sim 4.8 \text{ \AA pixel}^{-1}$. LRIS has a single Tektronix 2048 \times 2048 pixel CCD, which was binned in the spatial direction by a factor of 2 yielding $0.43'' \text{ pixel}^{-1}$.

A first set of exposures was obtained with the order blocking filter GG495, which is transmissive only at wavelengths greater than $\sim 0.48 \mu\text{m}$. This order-blocking filter is necessary to prevent the second-order blue part of the spectrum from overlapping the first-order red spectrum. Without the blocking filter, only wavelengths shorter than about $0.74 \mu\text{m}$ are uncontaminated. With the blocking filter, wavelengths from 0.48 to $0.96 \mu\text{m}$ can be observed without appreciable contamination. Two exposures of 295 s each were taken.

Immediately afterward, without repositioning the telescope, we took three internal (quartz lamp) flatfield exposures and one exposure with the Xe-Ar lamps to provide the wavelength calibration. The standard spectrophotometric calibrator HD 84937 ($V = 8.3$ mag, F5V, Oke & Gunn (1983)) was observed with the same settings to provide the spectral response of the spectrograph at an airmass of 1.12, within 10% of the airmass for WD 0346+246. The position angle for the slit was chosen to be the parallactic angle to minimize the effects of atmospheric dispersion (Filippenko 1982).

The second set of data was taken with the same grating and slit settings, but without the blocking filter. Again two 295 s exposures were obtained along with corresponding internal flatfields and arc lamp exposures. The same standard star was also observed in this manner.

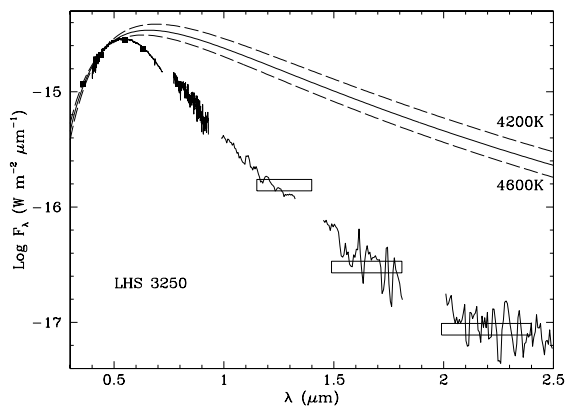


Fig. 2.— Spectra and photometry of LHS 3250. The notation and symbols are identical to those used in Figure 1. The optical photometry and the optical spectrum come from Harris et al. (1999).

In order to be certain that the spectrum near $1.0 \mu\text{m}$ was correct and uncontaminated, we obtained service observations with the same instrument settings on 24 December 1999 UT but with the RG850 blocking filter installed. This transmits wavelengths redward of $\sim 0.83 \mu\text{m}$, with the second-order contamination setting in at $2 \times 0.83 = 1.66 \mu\text{m}$. The weather was clear and the seeing was again $\sim 0.7''$. One 600 s exposure was taken, along with internal flatfields and arc lamp exposures. Because of the low sensitivity of the CCD in the near-infrared, these data are very noisy.

Using IRAF, we conducted standard CCD pro-

cessing and optimal spectral extraction, while flux calibration and telluric absorption band removal were done with our own routines in IDL. Final adjustments to the wavelength scale were obtained using the background sky regions.

The adopted reduction technique produces a spectrum which is flux calibrated independent of the photometric measurements. In this sense the spectrum differs from the infrared spectrum described above. The infrared spectrum is flux calibrated using the infrared photometry and the shape of a calibrator G star, which is not a spectrophotometric calibrator. In that case the G star is used only to provide the correct spectral shape, while the absolute calibration is provided by the infrared photometry. The spectrum presented in Figure 1 has a signal-to-noise ratio (S/N) over several hundred through the middle of the optical region. The infrared S/N falls from 2000 near $1 \mu\text{m}$ to approximately 6 in the K band.

The data taken on 15 December exhibits second-order contamination beyond $0.98 \mu\text{m}$, as shown by the uncontaminated data taken on 24 December. However, the infrared spectrum from NIRC has a much higher S/N, and the 24 December LRIS spectrum agrees perfectly with it, so we simply cut the optical spectrum at $0.97 \mu\text{m}$. Thus, in Figure 1, the data redward of $0.97 \mu\text{m}$ are from NIRC.

The optical photometry of WD 0346+246 presented in Hodgkin et al. (2000) and Hambly et al. (1997) was derived from CCD images made at the Jacobus Kapteyn Telescope. The B -band measurement only provided an upper limit and there was no U -band measurement. We have subsequently obtained U and B band CCD images of WD 0346+246 with the Palomar 1.5-m Oscar Meyer telescope and a Tektronix 2048×2048 pixel thinned, AR-coated CCD along with Johnson U and B filters. The pixel scale was $0.37'' \text{ pixel}^{-1}$, and the seeing on 10 and 11 August 1999 UT was $1.0''$ under photometric conditions.

On 10 August we obtained five 600 s exposures of the WD 0346+246 field. Each exposure was shifted by $10''$ in one of the cardinal directions from the previous exposure to minimize the effects of bad pixels. The Landolt (1992) standard field SA 112 was also observed with two 7 s exposures such that stars 250, 223, and 275 were in the field of view.

On 11 August 1999, we observed WD 0346+246 again but with the U filter. Four 1200 s exposures were made with dithering procedures similar to those described above. For U -band photometric standards we observed the Landolt (1992) field SA 110 and obtained images of stars 496, 497, 499, 502, 503, 504, 506, and 507 in two 60 s exposures.

Data were reduced by subtracting a median of five dark frames obtained on each night and dividing by flatfield exposures made by exposing the CCD to the illuminated dome. To obtain accurate photometric measurements of the white dwarf, we averaged the measurements of all the standard stars visible in each of the two calibration fields separately.

2.2. LHS 3250

Harris et al. (1999) presented the optical spectrum of LHS 3250 in the range 0.4 to 0.7 μm , as well as optical and infrared photometry (reproduced in Figures 2 and 3). To explore the SED in more detail beyond 0.7 μm , we obtained optical and infrared spectroscopy.

We measured the 0.75 to 0.98 μm spectrum of LHS 3250 through service observations at the William Herschel Telescope in the Canary Islands. The low resolution spectrum was obtained using the ISIS spectrograph with the R158R grating giving a wavelength scale of 2.9 \AA pixel $^{-1}$ over 2970 \AA on the TEK2 1024 \times 1024 pixel detector. The weather was good during the observations, and the seeing was measured to be 1". A 1" slit was employed. Two exposures, one of 1800 s and one of 1500 s, were taken on the target. These were bracketed by exposures of the spectrophotometric standard Ross 640. Calibration exposures of a tungsten flat (for flatfielding) and Cu-Ar and Cu-Ne arc lamps (for wavelength calibration) were also made. CCD data reduction, optimal spectral extraction, and flux calibration were performed using IRAF tasks.

We also observed LHS 3250 on 21 July 1999 UT using the Keck I 10-m telescope and NIRC (Matthews & Soifer 1994). We obtained Z_{CIT} , J , H , and K -band spectra spanning 1.0 to 2.5 μm .

The spectra were obtained at airmass ~ 1.4 during a photometric night with 0.3" seeing in K band. We used two different settings. The first measured the Z_{CIT} , J , and H bands simultane-

ously using the 150 l mm $^{-1}$ grism and the JH blocking filter. The slit was 0.3" wide. We obtained four exposures of 250 s with the white dwarf placed at two different positions in the slit.

The H and K band spectra were obtained simultaneously with the second setting. We used the same slit, the HK blocking filter and the 120 l mm $^{-1}$ grism. We obtained five exposures of 200 s each, again placing the white dwarf in one of two slit positions for each exposure.

The F8V star SAO 17455 ($V = 9.58$ mag) was observed with the same settings immediately after LHS 3250 to serve as a standard at an airmass of 1.4, matched to the LHS 3250 observations within 1%. For the first setting we obtained two 4.1 s exposures and for the second setting three 4.1 s exposures.

Data reduction followed our standard procedure. We first subtracted pairs of images from each other to remove the sky background. Using the optimal extraction technique we then reduced the spectra to one dimension. These steps were carried out on both the object and standard star spectra. After calibrating the wavelength scale, using the well-defined edges of the filter transmission curves (a technique good to an accuracy of 0.006 μm over the band), we summed the LHS 3250 spectra and divided by the standard star spectra. This removes the pixel-to-pixel variations and accounts for the instrumental sensitivity as a function of wavelength. A model F star spectrum was then divided into the resultant spectra.

3. Summary of Observations of Ultracool White Dwarfs

Figures 1 and 2, and Table 1, summarize the observations from §2. To provide a means of comparison, Figure 3 shows the spectra of LHS 3250, WD 0346+246, and F351–50 (from Ibata et al. (2000)). All of the white dwarf spectra are smooth and exhibit no fine features. The most important aspect of this figure is the fact that the three white dwarf spectra deviate from the black body spectrum redward of 0.6 μm . For reference a 4000 K black body spectrum is plotted at the top of the figure. The spectra are arranged in order of what we believe to be decreasing effective temperature, from top to bottom. (See §5 for a complete discussion of this.) Figure 3 also shows that

the peak wavelength appears to move toward red-der wavelengths, as the temperature drops, until WD 0346+246. Proceeding to cooler temperatures then moves the peak to *bluer* wavelengths. F351–50 appears on this plot because it is intrinsically faint (Ibata et al. 2000) and it exhibits a sudden change in spectral slope at $0.8 \mu\text{m}$. According to models (Saumon & Jacobson (1999); see §6), this may be the blue edge of the second vibrational band of the H_2 CIA. Other than this feature, the spectrum of F351–50 is almost identical to that of WD0346+246. The *BVR* colors are the same for these two objects. Without infrared photometry or a parallax it is difficult to make more concrete statements.

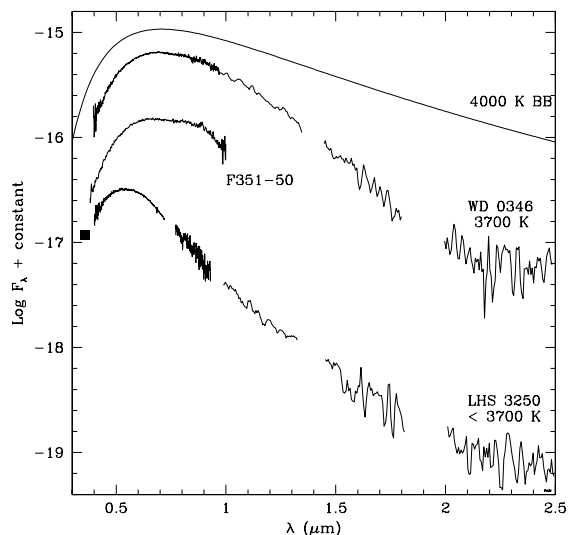


Fig. 3.— Comparison of spectra of cool halo white dwarfs; see §3 for a discussion. The optical spectrum of LHS 3250 is from Harris et al. (1999) and the F351–50 spectrum is from Ibata et al. (2000).

4. Are These White Dwarfs Members of the Halo?

The tangential space motion of WD 0346+246 is extremely high at 170 km s^{-1} and in a direction such that its Galactic orbit cannot be circular and must be strongly inclined to the Galactic disk. The conclusion in Hodgkin et al. (2000) was that this object is clearly a member of the Galaxy’s halo, regardless of what its unmeasurable radial velocity is.

Ibata et al. (2000) established that F351–50 must have a space velocity greater than 170 km s^{-1} and is therefore a member of the Galactic halo.

For LHS 3250 the case is not nearly as clear. Harris et al. (1999) demonstrated that the tangential velocity of LHS 3250 is $81.2 \pm 1.2 \text{ km s}^{-1}$. Unfortunately, LHS 3250 is essentially at 90° Galactic longitude and near the plane of the Galaxy. This, combined with the lack of any features in the spectrum that would permit measurement of the radial velocity, makes it impossible to determine whether it has a disk or halo orbit. However, there are several important features to note about the motion of LHS 3250 through the Galaxy. By subtracting the heliocentric motion from the velocities, it appears that LHS 3250 is moving toward the south Galactic pole at 73 km s^{-1} and toward the Galactic anticenter at 52 km s^{-1} . Thus the only definitive statement is that its orbit about the Galactic center cannot be circular. This makes LHS 3250 a probable member of the halo.

5. Physical Characteristics

In Hodgkin et al. (2000) we derived the radius, mass, luminosity and effective temperature of WD 0346+246. This derivation used a technique that exploits the brightness temperature of these objects as a function of wavelength. We have conducted an extensive series of tests of the technique and have found that it is not reliable. Here we describe the technique more explicitly than before, and we also explain why it is not viable.

In Hodgkin et al. (2000) the derivation of radius, mass, and effective temperature relied upon the distance, d , and the assumption that the bluest part of the optical spectrum behaves as a black body. By fitting this region with a known black body spectrum we believed that we could obtain the physical parameters. For pure H white dwarfs, the only known opacity in this wavelength region is due to H^- , which has a weak wavelength dependence in the optical regime. In pure He white dwarfs, the dominant opacity source in the optical is He^- , which is also very flat. The flatness of the opacity seemed to validate the technique. To support this argument, we examined plots of the brightness temperature vs. λ of synthetic spectra for pure hydrogen white dwarfs (Saumon & Jacobson 1999). Shown in Figure 4, these plots have

nearly constant brightness temperature in the visible part of the spectrum. For example, the brightness temperature of a $T_{\text{eff}} = 3500$ K, $\log g = 8$ model, where g is the surface gravity in cgs units, varies by less than 200 K from 0.4 to 0.9 μm . For white dwarfs with $T_{\text{eff}} \gtrsim 4500$ K, the SED is quite close to that of a black body.

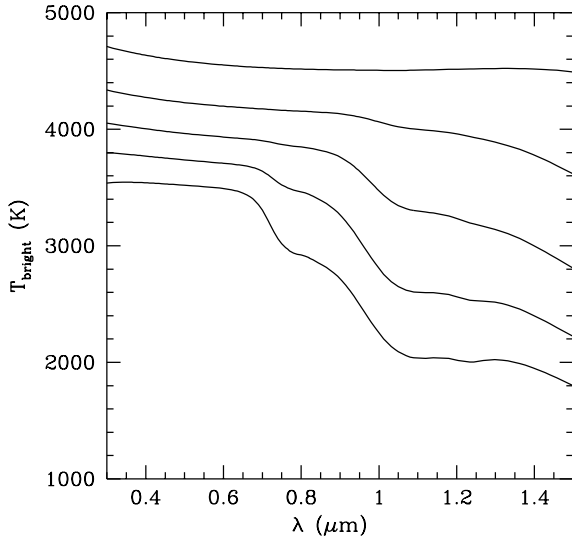


Fig. 4.— Brightness temperature as a function of wavelength from pure hydrogen synthetic spectra (Saumon & Jacobson 1999). All models have $\log g = 8$ and the effective temperature ranges from 4500 K to 2500 K in steps of 500 K, from top to bottom. In the cooler models, the strong drop of T_{bright} in the infrared is due to H_2 CIA absorption. Correspondingly, T_{bright} is significantly larger than T_{eff} at shorter wavelengths in these models. Note the virtual constancy of the brightness temperature at blue wavelengths.

To extract the radius of the star, then, involves fitting a black body curve, $B(T)$, to the optical region where the brightness temperature is nearly constant (below $\lambda = 0.5 \mu\text{m}$). The fit involves two parameters, the temperature of the black body fit and the ratio $(R/d)^2$. The temperature obtained from the fit is the brightness temperature in this region of the spectrum, not T_{eff} . Furthermore, the brightness temperature determines the shape of the black body curve, while the actual flux level is determined by $(R/d)^2$. Figures 1 and 2 show attempts to do this fitting on WD 0346+246 and LHS 3250.

Using this fitted temperature, T_{fit} , in each case, we derive the ratio R/d from the following equation: $(R/d)^2 \pi B_{U,B}(T_{\text{fit}}) = F_{U,B}$, where $F_{U,B}$ is

the flux in the fitted region from U to 0.5 μm , and $B_{U,B}(T_{\text{fit}})$ is the black body flux in the same wavelength region. For LHS 3250, this yields the result $R = 0.014 R_{\odot} \pm 0.002$, using the Harris et al. (1999) value of $d = 30.3 \pm 0.5$ pc. With the mass-radius relation from Chabrier et al. (2000) we find the mass to be $0.54 M_{\odot}$. For WD 0346+246, we derive $R = 0.013 R_{\odot} \pm 0.002$ and $M = 0.57 M_{\odot}$.

We can now determine the effective temperature from the relation $L = 4\pi R^2 \sigma T_{\text{eff}}^4$. By integrating all the flux measured from the U through K bands, we find for LHS 3250 $L = 3.26 \times 10^{-5} L_{\odot}$ and $T_{\text{eff}} = 3650$ K. Our value for L is somewhat higher than that derived by Harris et al. (1999), but it includes the important region of flux at 1 μm , for which they had no data. For WD 0346+246, we calculate $L = 1.83 \times 10^{-5} L_{\odot}$ and $T_{\text{eff}} = 3750$ K.

Criticism about the validity of this method prompted us to test it thoroughly. The white dwarf LHS 542 is an excellent test case since it has been analyzed by Leggett et al. (1998) by model fitting of the SED, an optical spectrum is available (Ibata et al. 2000) and the parallax is known. Our surface brightness method predicts a radius about 50% larger than the Leggett et al. (1998) solution. We have also performed a variety of tests using our new models (§6) to generate artificial, noiseless spectra (assuming R and d) and comparing the results of the surface brightness method with the input parameters of the synthetic data. We find that the method works very well when the brightness temperature of the star remains fairly constant over the wavelength interval of the fit. When the (monotonic) variation of the brightness temperature exceeds 100 K, however, the method becomes unreliable even though satisfactory fits of the spectrum can be obtained (Figures 1 and 2). The reason is that the derived value of T_{fit} over the interval is not an “average” or intermediate value in the range of brightness temperatures represented in the fitting interval. If T_{fit} were an intermediate value or average of the brightness temperature, the technique would be viable. The fact is that T_{fit} is systematically shifted *outside* of the actual range of brightness temperatures. This is due to the temperature dependence of the black body flux just blueward of the peak. The method thus converges to anomalous solutions for T_{fit} and R , solutions which deviate increasingly from the

actual values as the variation in brightness temperature increases. Since the degree of variation of the brightness temperature in an observed spectrum is *a priori* unknown, it is not possible to apply the method with confidence.

We conclude that the physical parameters of cool white dwarfs can only be obtained from fitting synthetic spectra to the observed SED.

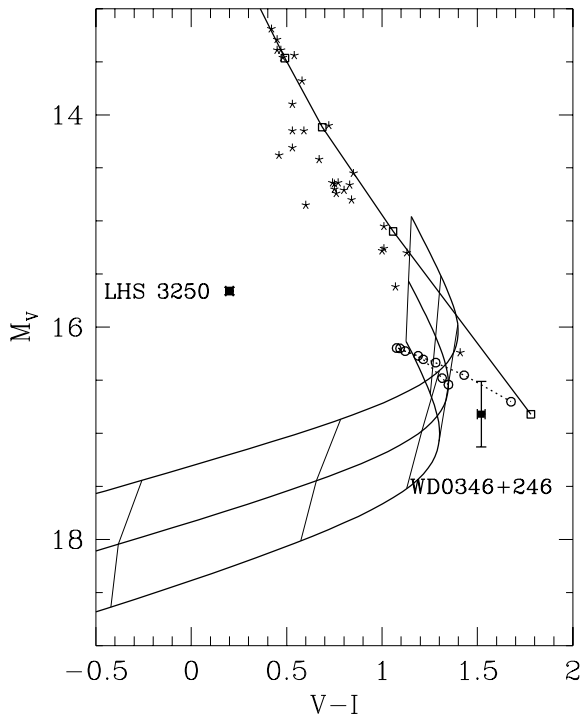


Fig. 5.— Hertzsprung-Russell diagram for cool white dwarfs. Solid lines connect the synthetic colors of pure hydrogen white dwarf atmospheres of a fixed gravity, with $\log g = 7.5, 8,$ and 8.5 from top to bottom. Thin lines connect those models which have the same T_{eff} , starting with $T_{\text{eff}} = 4500$ K right of center and decreasing in steps of 500 K. The open circles connected by a dashed curve show a sequence of atmospheres with mixed hydrogen and helium composition for $T_{\text{eff}} = 3500$ K and $\log g = 8$. Starting from the pure H model, the helium-to-hydrogen fraction $\log y = \log N(\text{He})/N(\text{H})$ increases from -1 to 7 in steps of 1. The colors of pure He atmospheres with $\log g = 8$ are shown by open squares connected with a solid line. The value of T_{eff} increases from 4000 to 7000 K in steps of 1000 K from bottom to top along this sequence. Star symbols represent cool, single white dwarfs with hydrogen-rich atmospheres as determined by Bergeron et al. (1997). The error bars on the M_V values include the uncertainty in the parallaxes of the stars.

6. Analysis of the Photometry

We can learn more about these stars by considering their locations in the Hertzsprung-Russell (HR) diagram (Figure 5) and in color-color diagrams (Figures 6 and 7). Synthetic spectra for white dwarf atmospheres of pure hydrogen and pure helium composition provide the means to interpret these diagrams. In Figures 5 to 7, we show a grid of pure hydrogen atmospheres (solid lines) with $\log g = 7.5, 8,$ and 8.5 (Saumon & Jacobson 1999), a sequence of pure helium atmospheres with $\log g = 8$ (Bergeron et al. 1995a) (open squares connected by a solid line), and stars from the cool white dwarf sample of Bergeron et al. (1997) which they identified as having a hydrogen-rich composition and which are not known or suspected of being binary (star symbols). Since very cool white dwarfs cool at constant radius, the sequences of constant gravity models shown in Figures 5 to 7 also represent cooling tracks. Along these pure H tracks, we can associate ages using new cooling models (Chabrier et al. 2000). Table 2 gives the ages for the intersection points on the solid-line grid in Figure 5.

Because neither WD 0346+246 nor LHS 3250 are explained by the pure H models, we found it necessary to consider models with mixed H/He atmospheres (indicated with open circles and dotted lines in Figures 5 to 7). These preliminary models have fixed values of T_{eff} and g and variable values of the relative abundance of He ($y = N(\text{He})/N(\text{H})$). These models allow the exploration of trends resulting from the general effects of mixed composition.

The qualitative behavior of the mixed H/He atmospheres can be deduced from Figure 15 of Bergeron et al. (1995a), which shows $B - V$ vs. $V - K$ for sequences of pure H, pure He, and mixed H and He composition with $y \leq 10$. As He is added to a cool H atmosphere of a given T_{eff} and surface gravity, the fractional abundance of H^- decreases, the relative importance of He- H_2 CIA opacity increases, and $V - K$ becomes bluer. This trend must reverse itself when y becomes very large, however, since both $V - K$ and $B - V$ of pure He models are very red (Figure 6). A sequence of models of fixed T_{eff} and g with composition varying from pure H to pure He is expected to become first very blue in $V - K$ at roughly constant $B - V$,

and then turn over to redder $B - V$ and $V - K$ until it reaches the colors of a pure He atmosphere.

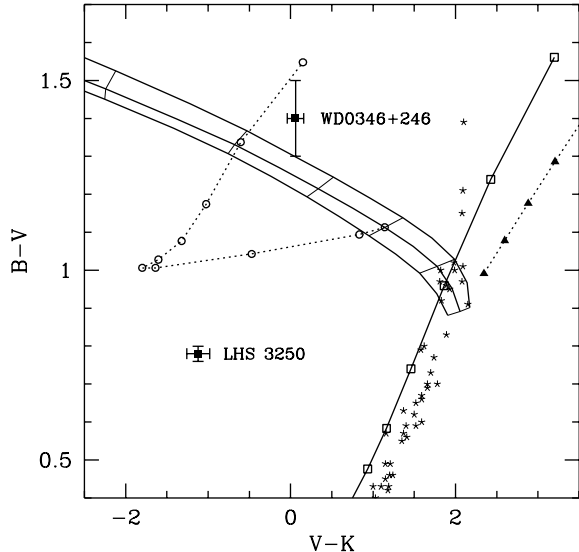


Fig. 6.— Color-color diagram for cool white dwarfs. See Figure 5 for an explanation of the symbols. The effective temperature along the hydrogen model grid decreases from 4500 K right of center to 2000 K toward the left in steps of 500 K. The colors of pure He atmospheres with $\log g = 8$ are shown by open squares. T_{eff} increases in steps of 500 K starting from 4000 K at the top. Triangles connected by a dotted line show the colors of black bodies starting with $T = 4500$ K at the bottom and decreasing in steps of 250 K. Compare with Fig. 15 of Bergeron et al. (1995b) or Fig. 9 of Bergeron et al. (1997).

Our preliminary sequence of mixed composition atmospheres varies the value of y over $0.1 \leq y \leq 10^7$ for a model with fixed $T_{\text{eff}} = 3500$ K and $\log g = 8$. This sequence is indicated by the open circles connected by dotted lines in Figures 5 to 7. These models are rather crude in their treatment of the chemical equilibrium and they ignore the non-ideal contributions to the equation of state which are significant for pure He atmospheres (Bergeron et al. 1995a). Nevertheless, they illustrate the qualitative behavior of mixed atmospheres and are adequate for the present purpose. It is readily apparent that the H_2 CIA reaches maximum strength for $\log y \approx 2 - 3$. However the colors of models of very large He abundance still differ significantly from those of pure He models because of a residual H_2 -He CIA opacity and He^- free-free opacity enhanced by the ionization of H. We find that in the BVK color-color diagram (Figure 6), very cool white dwarfs with

mixed H/He atmospheres occupy a much wider region than, and overlap with, the pure H atmospheres. Also, very cool white dwarfs with $J - H \lesssim -0.25$ have atmospheres of mixed H/He composition (Figure 7) and *do not* fall between the pure H and pure He sequences.

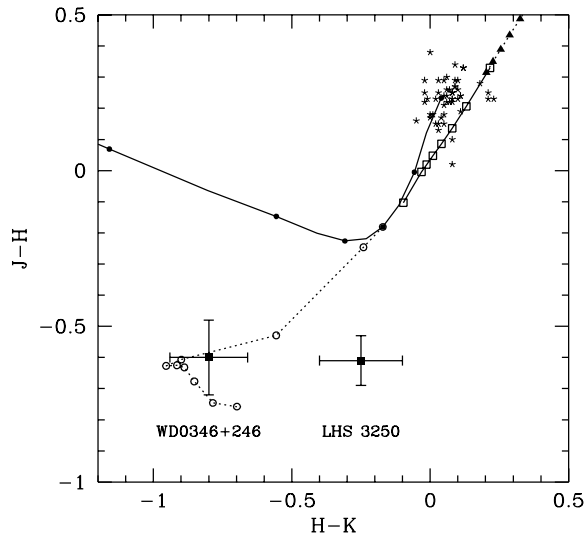


Fig. 7.— Color-color diagram for cool white dwarfs. Notation is the same as in Figure 5. Pure H models of different gravities very nearly overlap in this diagram, so we show only the $\log g = 8$ sequence for clarity. Filled circles indicate models with $T_{\text{eff}} = 4000$ K (upper right) and decreasing in steps of 500 K. Starting from the upper right, the open squares show the pure He sequence for $T_{\text{eff}} = 4000$ to 10000 K in steps of 1000 K, and $T_{\text{eff}} = 20000$ K at the top-right.

Figures 5 and 6 show that white dwarfs with atmospheres of pure He and pure H nearly overlap down to $T_{\text{eff}} \approx 3500 - 4000$ K. At these low values of T_{eff} , the CIA of H_2 becomes very strong and the hydrogen sequence turns over (Hansen 1999; Saumon & Jacobson 1999). The H-rich stars of Bergeron et al. (1997) reach down to the split between the two sequences. In the infrared (Figure 7), however, the two sequences overlap only for very different ranges of T_{eff} and are therefore easily distinguished. The HR diagram (Figure 5) is useful in assessing the evolutionary state of our objects, while the BVK diagram (Figure 6) provides a measure of the overall shape of the SED. Because CIA by H_2 gives rise to an opacity that is stronger in the infrared, its effects are dramatic in $V - K$.

The JHK color-color diagram (Figure 7) re-

TABLE 2
AGES OF PURE H, ULTRACOOOL WHITE DWARFS

T_{eff} (K)	$\log g = 8.5$	$\log g = 8.0$	$\log g = 7.8$
4500	11.7	8.6	6.0
4000	12.2	10.0	7.7
3500	12.6	11.1	9.2
3000	13.0	12.5	10.7
2500	13.3	13.6	12.1
2000	13.5	14.8	13.7

NOTE.—Ages are given in Gyr and correspond to the intersection points in the grid of solid curves in Figure 5. The last column corresponds to $\log g = 7.8$ while the bottom curve in Figure 5 is for $\log g = 7.5$. All of these ages are the result of new calculations (Chabrier et al. 2000) and are only pertinent to pure H atmospheres.

veals the shape of the SED in the infrared and is a most useful diagnostic of atmospheric composition of cool white dwarfs ($T_{\text{eff}} \lesssim 4500$ K). In this diagram, both the pure H and pure He sequences are insensitive to gravity. This confines atmospheres with pure compositions to two well-separated curves. Pure He atmospheres with $T_{\text{eff}} \lesssim 4500$ K are confined to the upper-right region of the diagram where $H - K > 0.15$ and $J - H > 0.25$, and their colors become redder for lower T_{eff} . On the other hand, pure H atmospheres have bluer colors with $H - K < 0.05$ and $-0.2 < J - H < 0.25$. The overlap of mixed H/He atmospheres with the pure composition atmospheres is very limited in the JHK diagram, and stars with $J - H < -0.25$ most certainly have mixed composition atmospheres.

Finally, we note that Bergeron et al. (1997) discuss the possibility of a continuum opacity source in pure H atmospheres which would affect the U and B bands. This helps in reproducing the $B - V$ color of the most extreme stars in their sample (the uppermost three stars in Figure 6). We have not included this opacity source in our models, however. The spectral fits described below were performed both with and without the U and B photometry; nearly identical results were obtained.

It is not presently possible to derive accurate

ages for very cool white dwarfs with pure He or He-rich atmospheres. However, as a point of reference we include in Table 2 ages of extremely cool, pure H white dwarfs. Correct treatments of helium pressure ionization, which determines the location of the photosphere of these objects, and of He^- absorption cross-sections at high densities, are lacking and prevent the derivation of reliable cooling curves for mixed-composition objects. The only certainty is that, because of their more transparent atmospheres, white dwarfs with He-rich atmospheres cool faster than their H-rich counterparts. For example, current models (Chabrier 1997) allow us to estimate that a pure He atmosphere, $0.6 M_{\odot}$ white dwarf will reach an effective temperature $T_{\text{eff}} = 4000$ K after only ~ 6 Gyr, much faster than cool DA white dwarfs. One should further note that even a small admixture of hydrogen or metals, due either to accretion or internal mixing processes, will slow down the cooling of the object dramatically, bringing it closer to a DA cooling sequence.

6.1. WD 0346+246

Figure 5 reveals that WD 0346+246 is intrinsically the faintest (in the V band) white dwarf known, with the exception of the high-mass degenerate ESO 439–26 (Ruiz et al. 1995). While

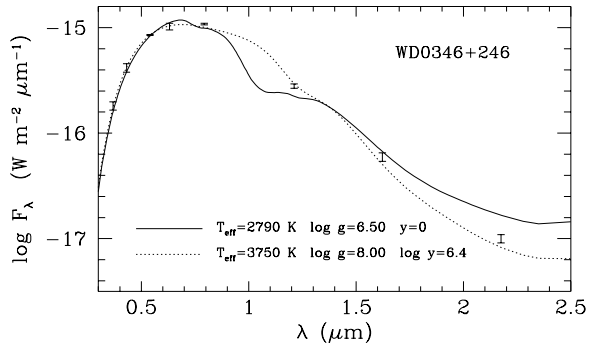


Fig. 8.— Fit of the U through K photometry of WD 0346+246. The broad-band photometric measurements (Table 1) are shown by $\pm 1\sigma$ error bars. The solid curve indicates the best-fit pure hydrogen atmosphere model with a gravity of $\log g = 6.5$. A slightly better fit can be obtained at even lower gravities. The dotted line is the best-fit mixed H/He atmosphere.

it is at the fork between the H and He cooling sequences, it does not obviously belong to either. Its BVK colors (Figure 6) reveal that it definitely does not have a pure He atmosphere. It does not sit on the pure H models either, except possibly with a very low gravity of $\log g \approx 6.5$ and $T_{\text{eff}} \approx 2700$ K. Indeed, a fit of pure hydrogen models to the broad-band photometry obtained by minimizing the error-weighted χ^2 gives $T_{\text{eff}} = 2790$ K for $\log g = 6.5$ (solid line in Figure 8). Since the distance of WD 0346+246 is known, the fit directly gives the radius of the star, $R = 0.0174R_{\odot}$. While our fit is fairly good, it is problematic in several ways. First, the optimal χ^2 and T_{eff} decrease slowly for even lower gravities. Such low values of T_{eff} and gravity would be rather extreme parameters for a white dwarf. Second, the slope of the fitted spectrum in the infrared is rather shallow and it misses the J and K photometry by 3σ to 4σ . Indeed, the $J-H$ color of WD 0346+246 (Figure 7) is ~ 0.5 mag bluer than both the sequences of pure H and pure He models. Third, the model spectrum predicts a strong CIA depression near $1 \mu\text{m}$ which is not present in the observed spectrum (Figure 1), indicating that pure hydrogen models are inappropriate.

We think that it is far more likely that the atmosphere of WD 0346+246 is of mixed hydrogen and helium composition. The colors of WD 0346+246 can be interpreted as those of a mixed H/He atmosphere based on Figures 5 through 7.

This is particularly supported by its $J-H$ color (Figure 7). Using a very limited grid of mixed composition atmospheres with $T_{\text{eff}} = 3500$ and 3750 K, $\log g = 8$, and $0 \leq y \leq 10^7$, we have fitted the He abundance to the observed broad-band fluxes of WD 0346+246. The result is shown by the dotted line in Figure 8. The fit of the photometry is excellent and the synthetic spectrum agrees remarkably well with our observed spectrum (Figure 1) at all wavelengths. We obtain a helium abundance of $\log y \approx 6.4$. Because the models are rather crude, this determination is inaccurate but it clearly indicates that the atmosphere contains only traces of hydrogen. The fitted radius is $R = 0.010 \pm 0.002R_{\odot}$. Finally, our choice of T_{eff} and $\log g$ for the mixed composition sequence appear to be reasonable estimates for WD 0346+246. From our analysis based on model atmospheres and spectra, we conclude that WD 0346+246 is a very cool white dwarf with $T_{\text{eff}} \approx 3700$ K, a typical surface gravity of $\log g \approx 8$, and a helium-dominated atmosphere ($5 \lesssim \log y \lesssim 8$).

6.2. LHS 3250

LHS 3250, on the other hand, stands apart from all other known white dwarfs in Figures 5 to 7. We can say with certainty that it does not have a pure He atmosphere. Its loci in each of these figures lead to contradictory interpretations. Figure 5 suggests that it is a very cool ($T_{\text{eff}} \approx 2400$ K), pure H or mixed H/He white dwarf. Its high V -band luminosity indicates that it either has a very low gravity and low T_{eff} , or high gravity with very high T_{eff} , or it may be a double degenerate. We can immediately exclude the high temperature possibility: its BVR colors are identical to those of WD 1656-062, which has a pure H atmosphere, $T_{\text{eff}} = 5520$ K and $\log g = 8$ (Bergeron et al. 1997). If it were this hot, however, it would show detectable $H\alpha$ absorption but it does not. Furthermore, its infrared colors would not be blue. Its BVK colors (Figure 6) can be understood if $T_{\text{eff}} \approx 4200$ K with a mixed H/He atmosphere dominated by He ($\log y \gtrsim 1$; see also Fig. 15 of Bergeron et al. (1995a)). Its infrared colors (Figure 7) suggest that it has a mixed H/He atmosphere dominated by He but with a very low temperature. Finally, our spectrum is featureless and the absence of a steep drop in the flux near $1.0 \mu\text{m}$ argues against significant H_2 CIA, but not

against He-H₂ CIA. It seems that neither pure H nor pure He atmospheres are sufficient to understand the nature of LHS 3250. Furthermore, Harris et al. (1999) were not able to fit its *V* through *K* photometry with either pure H or mixed H/He atmospheres. We have also failed with our new models and its SED remains unexplained.

A feasible solution to this problem may be that LHS 3250 is an unequal mass binary, with one component similar to WD 0346+246 and the other much cooler. This would have the effect of amplifying the optical flux, as compared to a single white dwarf, while contributing minimal amplification in the infrared. Until the full grid of mixed H/He models has been calculated, a synthetic, composite spectrum of such a combination is not forthcoming. We can only conclude that T_{eff} is below 4000 K, and, based on the severity of the 0.6 to 2.5 μm absorption, we suggest that it must be cooler than WD 0346+246 with $T_{\text{eff}} \approx 3700$ K.

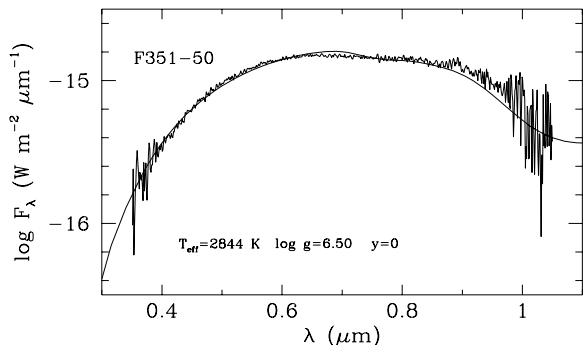


Fig. 9.— Fit of the spectrum of F351–50 by Ibata et al. (2000) with a pure hydrogen atmosphere.

6.3. F351–50

We have analyzed the 0.35 to 1.05 μm spectrum of F351–50 obtained by Ibata et al. (2000). Unfortunately, this part of the spectrum is not very sensitive to differences in surface composition. However, the presence of CIA, and hence of a significant amount of H, is suggested by the apparent change in the slope of the spectrum for $\lambda > 0.95 \mu\text{m}$. Although this is a very noisy part of the spectrum, we obtain an excellent fit with pure hydrogen models (Figure 9). The fitted parameters are $T_{\text{eff}} = 2844$ K and $\log g = 6.5$. These are extreme and unlikely parameters for a white dwarf and we attach only modest significance to

the result, for the same reasons that a similar fit to WD 0346+246 was not adequate.

The *BVRI* colors of F351–50 are nearly identical to those of WD 0346+246, suggesting that it may have a similar composition. If we ignore the part of the spectrum beyond 0.95 μm , where the S/N declines dramatically, we obtain an equally good fit with our restricted grid of mixed H/He composition atmospheres with $T_{\text{eff}} = 3500$ K, $\log g = 8$, and $\log y = 5.85$. As in the case of WD 0346+246, we find that mixed composition models lead to less extreme physical parameters. A more definitive analysis will require infrared photometry or the parallax of F351–50.

7. Conclusion

WD 0346+246 appears to be the first very cool white dwarf with an atmosphere of mixed hydrogen and helium composition. It has an effective temperature below 4000 K and shows only traces of hydrogen in its atmosphere. Only three other cool white dwarfs are known to have significantly high $N(\text{He})/N(\text{H})$ ratios. All three are in the C₂H spectral class and have $T_{\text{eff}} > 5300$ K (Bergeron et al. 1997). Although the spectral coverage of the available data is more limited for F351–50, it appears to be very similar to WD 0346+246. These two stars are the first examples of very cool white dwarfs with extremely high He to H mixing ratios and may provide important clues in understanding the spectral evolution of old white dwarfs.

The computation of an extensive and physically sound grid of mixed composition atmospheres for $T_{\text{eff}} \lesssim 5000$ K is necessary to obtain reliable determinations of the surface parameters for WD 0346+246 and F351–50. Such a grid of models may provide a better understanding of the intriguing white dwarf LHS 3250, which remains inscrutable.

We thank S. R. Kulkarni and J. S. Bloom for their support of this work, M. Irwin for providing us with his spectral data on F351–50, I. N. Reid for sharing the spectrum of LHS 3250 and J. Liebert for useful discussions and suggestions. We also graciously thank the two referees for a thorough job and for insisting that we check the technique in §5. Financial assistance for this work was provided by NASA through Hubble Fellowship

grant HF-01122.01-99A from the Space Telescope Science Institute, which is operated by the Association of Universities for Research in Astronomy, Inc., under NASA contract NAS5-26555. BRO acknowledges FUTDI. DS and AVF are supported by NSF grants AST-9731438 and AST-9987438, respectively. STH acknowledges the support of the Particle Physics and Astronomy Research Council. ALC is grateful for a National Science Foundation Graduate Research Fellowship. Part of this work was done under the auspice of the ALLIANCE project #00193 RL between the United Kingdom and France. The William Herschel Telescope is operated on the island of La Palma by the Isaac Newton Group in the Spanish Observatorio del Roque de los Muchachos of the Instituto de Astrofísica de Canarias. The W. M. Keck Observatory is operated as a scientific partnership among the California Institute of Technology, the University of California and NASA; it was made possible by the generous financial support of the W. M. Keck Foundation.

REFERENCES

- Bergeron, P., Ruiz, M.-T., Leggett, S. K., Saumon, D. & Wesemael, F. 1994, *ApJ*, 423, 456
- Bergeron, P., Saumon, D., & Wesemael, F. 1995a, *ApJ*, 443, 764
- Bergeron, P., Wesemael, F., & Beauchamp, A. 1995b, *PASP*, 107, 1047
- Bergeron, P., Ruiz, M.-T., & Leggett, S. K. 1997, *ApJS*, 108, 339
- Borysow, A., & Frommhold, L. 1990, *ApJ*, 348, L41
- Chabrier, G. 1997, in *IAU Symposium No. 189: Fundamental Stellar Properties*, ed. T. R. Bedding, et al. (New York: Kluwer), p. 381
- Chabrier, G., Brassard, P., Fontaine, G., & Saumon, D. 2000, *ApJ*, in press
- Filippenko, A. V. 1982, *PASP*, 94, 715
- Hambly, N. C., Smartt, S. J., & Hodgkin, S. T. 1997, *ApJ*, 489, L157
- Hambly, N. C., Smartt, S. J., Hodgkin, S. T., Jameson, R. F., Kemp, S. N., Rolleston, W. R. J., & Steele, I. A. 1999, *MNRAS*, 309, L33
- Hansen, B. 1999, *Nature*, 394, 860
- Harris, H. C., Dahn, C. C., Vrba, F. J., Henden, A. A., Liebert, J., Schmidt, G. D., & Reid, I. N. 1999, *ApJ*, 524, 1000
- Hodgkin, S. T., Oppenheimer, B. R., Hambly, N. C., Jameson, R. F., Smartt, S. J., & Steele, I. A. 2000, *Nature*, 403, 57
- Ibata, R., Irwin, I., Bienaymé, O., Scholz, R., & Guibert, J. 2000, *ApJ*, 532, L41
- Landolt, A. U. 1992, *AJ*, 104, 340
- Leggett, S. K., Ruiz, M.-T. & Bergeron, P. 1998, *ApJ*, 497, 294
- Matthews, K., & Soifer, B. T. 1994, in *Infrared Astronomy with Arrays: The Next Generation*, ed. I. S. McLean (New York: Kluwer), p. 239
- Oke, J. B., Cohen, J. G., Carr, M., Cromer, J., Dingizian, A., Harris, F. H., Labrecque, S., Luginio, R., Schaal, W., Epps, H., & Miller, J. 1995, *PASP*, 107, 375
- Oke, J. B., & Gunn, J. E. 1983, *ApJ*, 266, 713
- Ruiz, M. T., Bergeron, P., Leggett, S. K., & Anguita, C. 1995, *ApJ*, 455, L159
- Saumon, D., & Jacobson, S. 1999, *ApJ*, 511, L107